Evaluation of memory capacity and time series prediction using a spin Hall oscillator as reservoir

Arun Jacob Mathew[1], John Rex Mohan[1], Ruoyan Feng[1], Rohit Medwal[2], Surbhi Gupta[2], Rajdeep Singh Rawat[2], Yasuhiro Fukuma[1,3]

[1]Department of Physics and Information Technology, Faculty of Computer Science and Systems Engineering, Kyushu Institute of Technology, Iizuka 820-8502, Japan
[2]Natural Sciences and Science Education, National Institute of Education, Nanyang Technological University 637616, Singapore
[3]Research Center for Neuromorphic AI hardware, Kyushu Institute of Technology, Kitakyushu 808-0196, Japan

Spintronic devices, such as spin Hall oscillators and spin transfer torque oscillators, have become popular candidates for use as the reservoir in the reservoir computing architecture. The memory capacity of a reservoir quantifies the amount of information retained at any given time, indicating its significance for different reservoir computing tasks. In this work, we consider a spin Hall oscillator, consisting of a bilayer structure of platinum/permalloy, as the reservoir. Using micromagnetic simulations, we evaluate the change in memory capacity of the spin Hall oscillator system as the magnetization dynamics varies from transient state oscillations to limit cycle oscillations. We also perform a three-bit parity task to study the performance of the oscillator in carrying out a nonlinear task. A time series prediction task, namely the NARMA2 task, is also performed. The results of both tasks confirm a correlation between the evaluated memory capacity of the reservoir and its efficiency in performing temporal tasks. The best performance in reservoir computing tasks is observed when the output magnetization dynamics of the oscillator consists of both transient state and limit cycle oscillations.

***Index Terms* — Memory capacity, nonlinear magnetization dynamics, reservoir computing, spin Hall oscillators.**

I. Introduction

Today, the use of Artificial Neural Networks (ANNs), for performing computational tasks, has become common [1]. Their inherent complexity in structure, due to multiple hidden layers and their associated weights, enables ANNs to perform the most difficult computational tasks with great success. Reservoir Computing (RC), a computation scheme derived from traditional ANNs, has been gaining popularity as it can be implemented easily using physical devices [2]-[4]. The RC scheme offers a significant reduction in training cost as compared to traditional ANNs, since only the weights at the readout (W_{out}) connecting the reservoir and output layers, need to be trained [5]. Furthermore, with the weights of the intermediate layers not requiring any adaptive update, there is an increased freedom in the choice of reservoir [6]. The suitability of a possible reservoir in performing a particular computation task can be quantified in terms of the memory contributed by the reservoir [7]. Memory Capacity (MC) is a measure of the short term memory possessed by a reservoir [5]. In other words, it signifies how much information about a previous input is contained in the present output of the reservoir. A finite value of MC may be given by a simple linear network too. Therefore, in addition to the linear MC evaluation, it becomes necessary to confirm the nonlinear nature of the reservoir's memory by performing a nonlinear task, such as a three-bit parity check (PC) [8].

A wide range of physical systems, such as electronic, photonic, mechanical and spintronic systems are being investigated as possible RC candidates [9]. In particular, the small size (orders of nm), energy efficiency (orders of nJ) and rich dynamics of spintronic devices make them highly suitable for carrying out complex computations [10]. Spintronic oscillators such as Spin Torque Oscillators (STOs) and Spin Hall Oscillators (SHOs) are being actively investigated in this direction. STOs utilize a spin polarized current, generated using one ferromagnet, to affect magnetization dynamics in another ferromagnet [11]-[12]. Meanwhile, in SHOs, a pure spin current is generated in a nonmagnetic layer, which can be utilized to affect the magnetization dynamics of the adjoining magnetic layer [13]-[14]. STOs based on magnetic tunnel junctions, have been used to perform character [15] and audio [16] recognition tasks. However, in STO devices, the spin polarized current used can lead to significant energy loss in the form of heating. Using the SHO which utilizes pure spin current, we can perform all computations carried out using an STO, in a significantly more energy efficient manner [17]-[18].

In this work, we perform micromagnetic simulations of a SHO structure, and utilize the magnetization dynamics as the reservoir output in performing various RC benchmark tasks. Different kinds of dynamics such as transient oscillations and limit cycle oscillations are excited in the SHO by varying the input parameters, namely the input current amplitude and pulse width. It is essential to understand how the performance of the reservoir changes with the kind of dynamics that is

excited in the oscillator, because in the RC scheme we do not have any other control parameters to effect the working of the reservoir [4]. We evaluate the MC of the SHO reservoir as a function of the input parameters. We also perform a PC task to confirm the nonlinearity in the reservoir. Finally, we carry out a time series prediction task, namely, the Nonlinear Auto Regressive Moving Average (NARMA) task [19], and evaluate the performance of the reservoir as a function of the input parameters.

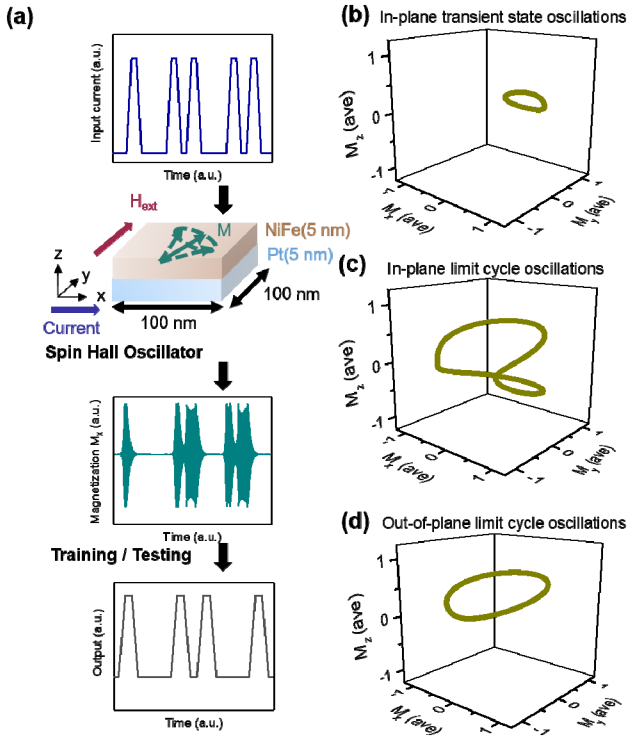

Figure 1: (a) Schematic diagram showing the use of a spin Hall oscillator as the reservoir in performing a computation task. Depending on the input current amplitude and pulse width, **(b)** in plane transient oscillations, **(c)** in plane limit cycle oscillations, or **(d)** out of plane limit cycle oscillations can be excited in the spin Hall oscillator.

II. Simulation Parameters

A general RC scheme with the SHO as the reservoir is shown in Fig. 1(a). Simulations were performed using LLG micromagnetic simulator [20]-[21]. A bilayer SHO structure having dimensions 100 nm × 100 nm × 10 nm, with platinum Pt (5 nm) as the bottom layer and permalloy NiFe (5 nm) as the upper layer, was considered. A single domain model was assumed in all our studies. The time evolution of the normalized magnetization $\vec{m}$ is solved by the Landau-Lifshitz-Gilbert (LLG) equation with inclusion of the Spin Transfer Torque (STT) term,

$$\frac{d\vec{m}}{dt} = -\gamma(\vec{m}\times\mu_0\vec{H}_{eff}) + \alpha\,(\vec{m}\times\frac{d\vec{m}}{dt}) - \gamma\frac{\hbar\theta_{SH}\,j_c}{2eM_S t_{NiFe}}(\vec{m}\times\vec{m}\times\vec{\sigma}), \qquad (1)$$

with gyromagnetic ratio γ, damping constant α, saturation magnetization M_S, reduced Planck constant $\hbar$, electron charge e and NiFe layer thickness t_{NiFe}. The effective field $\vec{H}_{eff}$ consists of the external magnetic field H_{ext}, magneto crystalline anisotropy field, exchange field and demagnetization field. The spin Hall angle θ_{SH} quantifies the conversion efficiency of charge current density j_c to spin current density j_s in the Pt layer. The direction of spin polarization σ is given by a cross product of the unit vectors of the spin and charge currents ,respectively. Depending on the magnitude and direction of j_c, the STT term in (1) competes with the damping term, leading to oscillation of the magnetization.

The charge current was applied along the x-axis, while an external magnetic field $\mu_0 H_{ext} = 100$ mT was applied along the y-axis as shown in the Fig. 1(a). The material parameters were chosen in agreement with experimentally obtained values [22]-[24], with saturation magnetization $\mu_0 M_S = 1.0$ T, damping constant $\alpha = 0.02$ and resistivities of $\rho_{NiFe} = 4.5\times10^{-7}\ \Omega$ m and $\rho_{Pt} = 2.0\times10^{-7}\ \Omega$ m for NiFe and Pt, respectively.

III. Results And Discussions

A. Magnetization dynamics of Spin Hall Oscillator (SHO)

Depending on the magnitude and pulse width of the input current, the magnetization dynamics can exhibit in-plane transient state oscillations (Fig. 1(b)), in-plane limit cycle oscillations (Fig. 1(c)) or out-of-plane limit cycle oscillations (Fig. 1(d)). We first investigate the magnetization dynamics induced by a single input current pulse as shown in Fig. 2(a). The pulse parameters t_{rise}, t_{fall} and t_{relax} are fixed at 1 ns and the pulse width t_{pw} is varied from 1 ns to 5 ns. The pulse period is denoted by T. The amplitude of the current pulse is given by I. We study the M_x component of magnetization as the output of the SHO in all analyses. This is because, experimental detection of the SHO oscillations is based on anisotropic magnetoresistance (AMR) which depends on the relative orientation between current and magnetization θ_{AMR} [25]. The oscillating term in AMR is directly proportional to θ_{AMR}, which in turn, is directly proportional to M_x. For a fixed t_{pw}, as current amplitude I increases, the amplitude of the oscillating M_x component is found to increase, as expected (Fig. 2(b)-(d)) [26]. A similar trend is observed as t_{pw} increases, for a fixed I (Fig. 2(b), 2(e) and 2(f)). We observe that for a fixed t_{pw}, as I increases, the magnetization dynamics changes from a low amplitude transient state to a higher amplitude transient state. Eventually, at a high enough I, the oscillation amplitude saturates and reaches the limit cycle. As I is increased further, the limit cycle oscillations become out of plane. Similarly, for

a fixed I, as t_{pw} increases, the dynamics similarly shifts from a transient state to in plane limit cycle oscillations and then to out of plane limit cycle oscillations. We observe that with the increase in either amplitude or pulse width, the magnetization dynamics of the oscillator moves from a state of transient dynamics at increasing amplitudes to in plane and then finally to out of plane limit cycle oscillations.

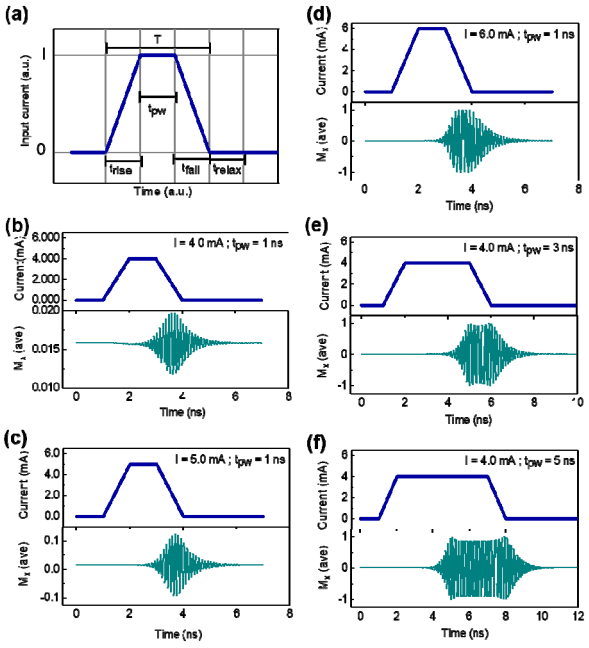

Figure 2: (a) Current pulses of different amplitude I and pulse width t_{pw} are given as input to the spin Hall oscillator. Single current pulses with **(b)** I = 4.0 mA; t_{pw} = 1 ns, **(c)** I = 5.0 mA; t_{pw} = 1 ns, **(d)** I = 6.0 mA; t_{pw} = 1 ns, **(e)** I = 4.0 mA; t_{pw} = 3 ns, and **(f)** I = 4.0mA; t_{pw} = 5ns, given as input to the spin Hall oscillator and the corresponding M_x oscillations induced by them.

B. Time series input for Reservoir Computing (RC) tasks

We proceed to investigate the magnetization dynamics when a stream of 1270 bits are fed as input current pulses to the SHO. Bit 0 is defined as the input current pulse with I=0. Bit 1 is the input current pulse having a finite amplitude I. The upper envelope of the oscillating M_x component (named S(t) henceforth) is used as the output corresponding to a particular input in all subsequent analyses. We define a quantity called delay d, and the S(t) corresponding to the k^{th} input bit is related to the $(k\text{-}d)^{th}$ input bit (Fig. 3(a)). The input current pulses and the corresponding output M_x oscillation and its upper S(t) are shown for different sets of I and t_{pw} in Figs. 3(b)-(f). From Figs. 3(b)-(d), we find that for a particular value of t_{pw}, as I increases, the value of the corresponding S(t) also increases for the same input bit. For a particular value of I, a similar increase in S(t) is seen with the increase in t_{pw}, as shown in Figs. 3(b), 3(e) and 3(f). At lower values of I and t_{pw}, even when multiple finite pulses are consecutively given as input, the output S(t) remains in the transient state with increasing amplitude with each input pulse. As I or t_{pw} is increased, limit cycle oscillations are observed after multiple consecutive input pulses. This results in a combination of transient and limit cycle oscillations in the output S(t). When I or t_{pw} is sufficiently high, all oscillations are in the limit cycle. Having seen the variation in the output dynamics of the SHO with change in amplitude and pulse width of the multiple input current pulses, we proceed to utilize the output S(t) of the SHO for performing various reservoir computing benchmark tasks.

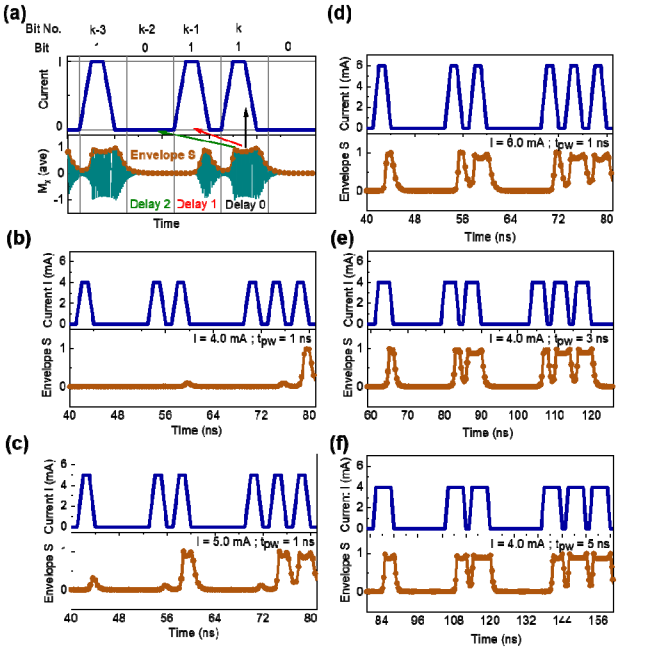

Figure 3: (a) Five bits (10110), from a total number of 1270 bits, given as input to the spin Hall oscillator. The M_x oscillations and their upper envelope S(t) for I = 5.5 mA, t_{pw} = 1 ns. In memory capacity calculations, nodes of S(t) are trained to reproduce a particular input bit depending on the delay. Multiple current pulses with **(b)** I = 4.0 mA; t_{pw} = 1 ns, **(c)** I = 5.0 mA; t_{pw} = 1 ns, **(d)** I = 6.0 mA; t_{pw} = 1 ns, **(e)** I = 4.0 mA; t_{pw} = 3 ns, and **(f)** I = 4.0mA; t_{pw} = 5ns, given as input to the spin Hall oscillator and the corresponding upper envelopes S(t) induced by them.

C. Memory Capacity (MC)

First, S(t) is discretized into N nodes for each input bit. The i^{th} node for the envelope S(t) corresponding to the k^{th} input bit is given by,

$$S_{k,i} = S((k-1)T + i(\frac{T}{N})), \qquad (2)$$

where index $i = 0, 1, \ldots, N$ and index $k = 0, 1, \ldots, 1270$. The weight $w_{d,i}$ is defined as satisfying the relation,

$$\sum_{i=1}^{N+1} w_{d,i} S_{k,i} = b(k-d), \qquad (3)$$

where $b(k-d)$ is the $(k\text{-}d)^{th}$ input bit. The $(N+1)^{th}$ term in the discretized output S corresponds to a constant bias term, and is fixed to be unity. For a finite value of d in (2), $S_{k,i}$ is related to the input bit $b(k-d)$, which is d steps in the past. Equation (3) can be written in matrix form as given below,

$$WS = B. \quad (4)$$

Solving for W using the Moore-Penrose pseudo inverse method [27], we get,

$$W = (S^T S + \lambda I)^{-1} S^T B, \quad (5)$$

where λ is the regularization constant (fixed at 1×10^{-5}). After optimization of W using the training set of input bits B and output envelope S, the weight matrix W and the testing output envelope S' are used to predict the testing set of input bits denoted by B'.

$$B'_{rep} = WS'. \quad (6)$$

The quality of prediction is quantified by the correlation coefficient $C(d)$ defined as,

$$C(d) = \frac{\mathrm{cov}[(B'_{rep}, B')]^2}{\mathrm{var}(B'_{rep})\,\mathrm{var}(B')}, \quad (7)$$

with the functions cov and var indicating the covariance and variance of the associated quantities. Memory capacity MC is defined as the sum of $C^2(d)$ over all range of delays d, given by,

$$MC = \sum_{d=1}^{d_{max}} C^2(d), \quad (8)$$

where d_{max} is fixed as 10.

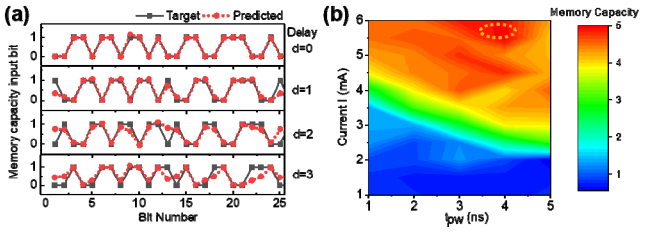

Figure 4: (a) Target and predicted inputs of the memory capacity task, for the first 25 bits out of the 420 bits of training data (N=10, regularisation constant λ=1e-5, I = 5.5 mA, t_{pw}=1 ns). Note that with increasing delay, the difference between the target and predicted values increases **(b)** Color map showing the memory capacity as a function of input amplitude I and and pulse width t_{pw}.

Fig. 4(a) shows the target and predicted data for the first few testing input bits. We see that, as the delay d increases, the difference between the target and predicted data also increases. This indicates that, as we move further back in the past, the SHO output retains lesser information regarding the input. We calculate MC for different values of t_{pw} and I. The MC values obtained for the various combinations of t_{pw} and I are depicted as a color map in Fig. 4(b). As shown in Fig. 4(b), when t_{pw} is fixed and I is increased, we observe a difference in the magnetization dynamics that contributes to the MC. For lower values of I, all output oscillations remain in the transient state and hence corresponding MC values are also low. As I is increased, limit cycle oscillations too start to contribute for inputs of continuous input bit 1 pulses. At sufficiently high I, all output oscillations are limit cycle oscillations and hence the maximum possible value of MC is obtained. A similar trend is seen for a fixed I and increase in t_{pw}. MC is found to saturate in the range of 4.5 to 5.0. Any further increase in I or t_{pw} does not increase MC. The reason for the saturation of MC in this range is due to the dynamics approaching the limit cycle of oscillations for all pulses. The input parameters at which limit cycle oscillations are reached are determined by the inherent time scales of the oscillations and their relaxation for the SHO, which is of the order of few ns.

The highest value of MC = 5.0 is found for I = 5.5 mA and t_{pw} = 4 ns. For higher values of I or t_{pw}, the MC is found to be lower. We can infer that when more out of plane limit cycle oscillations contribute to the output of the SHO reservoir, there is a decrease in the memory of the reservoir. This decrease in MC can be attributed to the magnetization precessing about an axis different from the in plane easy axis of the ferromagnet. Higher values of MC are seen when the oscillation dynamics includes transient state oscillations and in plane limit cycle oscillations.

D. Three-bit Parity Check (PC)

When performing PC, the target function changes from $b(k-d)$, modifying (3) as given below,

$$\sum_{i=1}^{N+1} w_{d,i} S_{k,i} = [\sum_{j=d}^{d-2} b(k-j)] (\mathrm{mod}\, 2). \quad (9)$$

All other calculations remain same as that for MC. We compare the predicted output B'_{rep} with the theoretical output B', in terms of the Normalized Mean Square Error (NMSE), given by,

$$NMSE = \frac{\sum_i (B'_{rep,\,i} - B_i')^2}{\sum_i (B_i')^2}. \quad (10)$$

The color map in Fig. 5(a) gives the NMSE of the three-bit parity task for various combinations of t_{pw} and I. We observe similar trends as observed for MC. When fixing t_{pw} and increasing I, and vice-versa, the NMSE is found to decrease. From Fig. 4(b) and Fig.5(a), we see that the least NMSE in three-bit PC is found in the same region which corresponds to highest MC. Thus, the high MC possessed by the reservoir is found to improve its performance in the three-bit parity task.

E. NARMA Tasks

Modelling a dynamical system is the most elegant way to evaluate the computational capability of any system [5]. For our SHO as reservoir, we carry out a time series prediction task, the Nonlinear Auto Regressive Moving Average (NARMA) task. In a NARMA task of order 2, we assume a nonlinear dynamical system that generates an output y_k based

on a second order nonlinear function defined as,

$$y_k = 0.4y_{k-1} + 0.4y_{k-1}y_{k-2} + 0.6u_k^3 + 0.1, \quad (11)$$

where u_k is the corresponding input in the range [0, 0.5]. Thus the output at any particular time depends on the corresponding input as well as the two previous outputs. For a reservoir to successfully replicate the second order nonlinear dynamical output given above in (11), it needs to have sufficient memory to retain information at least up to the two previous outputs [26]. The same 1270 bits used in the MC and PC tasks are fed as input to the SHO. We train our SHO reservoir to map the above function in (10), and evaluate the accuracy of the predicted output p_k with respect to the theoretical output y_k, again in terms of the NMSE, given by,

$$NMSE = \frac{\sum_i (y_i - p_i)^2}{\sum_i y_i^2}. \quad (12)$$

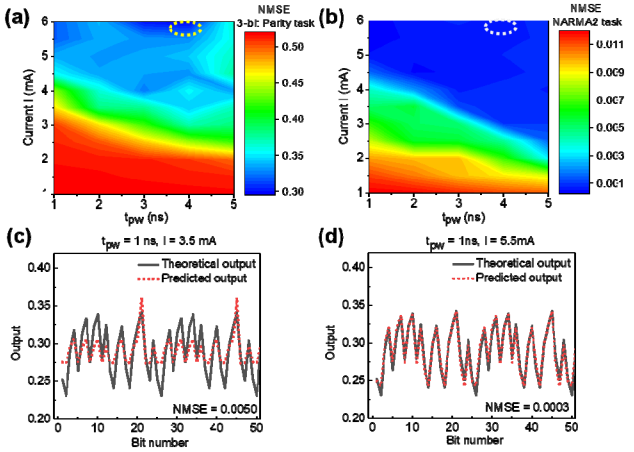

Figure 5: Color map showing the NMSE of **(a)** the three-bit parity task and **(b)** the NARMA2 task as a function of input amplitude I and pulse width t_{pw}. Theoretical and predicted outputs of the NARMA2 task for **(c)** I = 3.5 mA, t_{pw} = 1 ns and **(d)** I = 5.5 mA, t_{pw} = 1 ns.

With increasing I, there is better agreement between theoretical and predicted outputs seen by the decrease in NMSE value. NMSE for the NARMA2 task as a function of I and t_{pw} are shown in a color map in Fig. 5(b). The theoretical and predicted outputs for the NARMA2 task, with t_{pw}=1 ns, I = 3.5mA and t_{pw}=1 ns, I = 5.5mA are shown in Fig. 5(c) and Fig. 5(d) respectively. For a fixed value of I, as t_{pw} increases, the NMSE decreases. When t_{pw} is fixed, and I increased, again a decrease in NMSE is seen. Correlating the different color maps from Figs. 4(b), 5(a) and 5(b), we can infer that the decrease in NMSE of the NARMA2 task is due to the increase in the memory capacity of the SHO reservoir. As discussed previously, this increased MC corresponds to magnetization dynamics which includes both transient and in plane limit cycle oscillations, but not to out of plane limit cycle oscillations which decreases MC value. Thus, we are able to confirm that by enhancing its memory capacity, our SHO reservoir is able to improve its performance in the time series prediction task.

IV. Conclusion

We studied numerically, the effect of the magnetization dynamics of the spin Hall oscillator on its MC, when used in a reservoir computing scheme. The MC was found to improve with increase in input current pulse amplitude and pulse width, and eventually saturated in the range of 4.5 to 5.0 (Fig. 5(b)). This saturation can be correlated with the magnetic oscillations moving from a state of transient dynamics to in-plane limit cycle oscillations. Any further increase in amplitude or pulse width of the current pulse, corresponding to out-of-plane limit cycle oscillations, was found to decrease the memory capacity. The observed trend in MC was further confirmed to be due to the magnetization dynamics of the oscillator through the three-bit PC task, which showed minimum error for input parameters that correspond to the highest MC. Further, the SHO was used as a reservoir in performing NARMA2 time series prediction. The NMSE of the NARMA2 task was found to decrease with increase in the MC of the SHO, confirming a correlation between the calculated MC and the performance of the SHO reservoir in the NARMA2 task.

Acknowledgment

Y.F. would like to acknowledge JSPS Grant-in-Aid (KAKENHI No. 22K04198), KIOXIA Corporation and Iketani Science and Technology Foundation. R. S. R. would like to acknowledge the support from the Ministry of Education, Singapore grant no MOE2019-T2-1-058 (ARC 1/19 RSR) and National Research Foundation grant no NRF-CRP21-2018-0003.

References

[1] B. Goertzel, "Artificial General Intelligence: Concept, state of the art, and future prospects," *Journal of Artificial General Intelligence*, vol. 5, no. 1, pp. 1–48, 2014.

[2] W. Maass, T. Natschläger, and H. Markram, "Real-time computing without stable states: A new framework for Neural Computation based on perturbations," *Neural Computation*, vol. 14, no. 11, pp. 2531–2560, 2002.

[3] H. Jaeger and H. Haas, "Harnessing nonlinearity: Predicting Chaotic Systems and saving energy in wireless communication," *Science*, vol. 304, no. 5667, pp. 78–80, 2004.

[4] D. Verstraeten, B. Schrauwen, M. D'Haene, and D. Stroobandt, "An experimental unification of Reservoir Computing Methods," *Neural Networks*, vol. 20, no. 3, pp. 391–403, 2007.

[5] H. Jaeger, "The 'echo state' approach to analyzing and training recurrent neural networks," German Nat. Res. Center Inf. Technol., St. Augustin, Germany, GMD Rep. 148, 2001.

[6] G. Tanaka, T. Yamane, J. B. Héroux, R. Nakane, N. Kanazawa, S. Takeda, H. Numata, D. Nakano, and A. Hirose, "Recent advances in Physical Reservoir Computing: A Review," *Neural Networks*, vol. 115, pp. 100–123, 2019.

[7] K. Nakajima, "Physical Reservoir Computing—an introductory perspective," *Japanese Journal of Applied Physics*, vol. 59, no. 6, p. 060501, 2020.

[8] N. Bertschinger and T. Natschläger, "Real-time computation at the edge of chaos in recurrent neural networks," *Neural Computation*, vol. 16, no. 7, pp. 1413–1436, 2004.

[9] I. Fischer and K. Nakajima, Reservoir computing: Theory, physical implementations, and applications. Springer, 2021.
[10] J. Grollier, D. Querlioz, K. Y. Camsari, K. Everschor-Sitte, S. Fukami, and M. D. Stiles, "Neuromorphic Spintronics," *Nature Electronics*, vol. 3, no. 7, pp. 360–370, 2020.
[11] J. C. Slonczewski, "Current-driven excitation of magnetic multilayers," *Journal of Magnetism and Magnetic Materials*, vol. 159, no. 1-2, 1996.
[12] S. I. Kiselev, J. C. Sankey, I. N. Krivorotov, N. C. Emley, R. J. Schoelkopf, R. A. Buhrman, and D. C. Ralph, "Microwave oscillations of a nanomagnet driven by a spin-polarized current," *Nature*, vol. 425, no. 6956, pp. 380–383, 2003.
[13] V. E. Demidov, S. Urazhdin, G. de Loubens, V. Cros, A. Anane, S. O. Demokritov, "Magnetization oscillations and waves driven by pure spin currents", *Physics Reports*, vol. 673, pp. 1-31, 2017.
[14] S. Manna, R. Medwal, S. Gupta, J. R. Mohan, Y. Fukuma, R. S. Rawat, "Anisotropy-assisted bias-free spin Hall nano-oscillator", *Applied Physics Letters*, vol. 122, p. 072401, 2023
[15] K. Yogendra, D. Fan, and K. Roy, "Coupled spin torque nano oscillators for low power neural computation," *IEEE Transactions on Magnetics*, vol. 51, no. 10, pp. 1–9, 2015.
[16] J. Torrejon, M. Riou, F. A. Araujo, S. Tsunegi, G. Khalsa, D. Querlioz, P. Bortolotti, V. Cros, K. Yakushiji, A. Fukushima, H. Kubota, S. Yuasa, M. D. Stiles, and J. Grollier, "Neuromorphic computing with Nanoscale Spintronic Oscillators," *Nature*, vol. 547, no. 7664, pp. 428–431, 2017.
[17] M. Tarequzzaman, T. Böhnert, M. Decker, J. D. Costa, J. Borme, B. Lacoste, E. Paz, A. S. Jenkins, S. Serrano-Guisan, C. H. Back, R. Ferreira, and P. P. Freitas, "Spin torque nano-oscillator driven by combined spin injection from tunneling and spin hall current," *Communications Physics*, vol. 2, no. 1, 2019.
[18] E. Jué, W. H. Rippard, and M. R. Pufall, "Comparison of the spin-transfer torque mechanisms in a three-terminal spin-torque oscillator," *Journal of Applied Physics*, vol. 124, no. 4, p. 043904, 2018.
[19] A. F. Atiya and A. G. Parlos, "New results on recurrent network training: Unifying the algorithms and accelerating convergence," *IEEE Transactions on Neural Networks*, vol. 11, no. 3, pp. 697–709, 2000.
[20] A. Deka, I. Tanaka, J. R. Mohan, Y. Fukuma, "Modulation of Magnetization Precession Trajectories by Perpendicular Magnetic Anisotropy in CoFeB Thin Films", *IEEE Transactions on Magnetics*, vol. 56, no. 7, p. 4300205, 2020.
[21] A. Deka, K. Sato, I. Tanaka, Y. Fukuma, "Simulations on the Effect of Magnetic Anisotropy on Switching of an Easy Cone Magnetized Free Layer", *IEEE Transactions on Magnetics*, vol. 56, no. 3, p. 6702404, 2020.
[22] U. Shashank, R. Medwal, T. Shibata, R. Nongjai, J. V. Vas, M. Duchamp, K. Asokan, R. S. Rawat, H. Asada, S. Gupta, and Y. Fukuma, "Enhanced Spin Hall effect in s-implanted PT," *Advanced Quantum Technologies*, vol. 4, no. 1, p. 2000112, 2020.
[23] U. Shashank, R. Medwal, Y. Nakamura, J. R. Mohan, R. Nongjai, A. Kandasami, R. S. Rawat, H. Asada, S. Gupta, and Y. Fukuma, "Highly dose dependent damping-like spin–orbit torque efficiency in O-implanted PT," *Applied Physics Letters*, vol. 118, no. 25, p. 252406, 2021.
[24] U. Shashank, Y. Nakamura, Y. Kusaba, T. Tomoda, R. Nongjai, A. Kandasami, R. Medwal, R. S. Rawat, H. Asada, S. Gupta, Y. Fukuma, "Disentanglement of intrinsic and extrinsic side-jump scattering induced spin Hall effect in N-implanted Pt", *Physical Review* B, vol. 107, p. 064402 2023.
[25] R. H. Liu, W. L. Lim, and S. Urazhdin, "Spectral characteristics of the microwave emission by the Spin Hall Nano-Oscillator," *Physical Review Letters*, vol. 110, no. 14, 2013.
[26] A. Slavin and V. Tiberkevich, "Nonlinear auto-oscillator theory of microwave generation by spin-polarized current," *IEEE Transactions on Magnetics*, vol. 45, no. 4, pp. 1875–1918, 2009.
[27] R. Penrose, "A generalized inverse for matrices," *Mathematical Proceedings of the Cambridge Philosophical Society*, vol. 51, no. 3, pp. 406–413, 1955.
[28] W. Jiang, L. Chen, K. Zhou, L. Li, Q. Fu, Y. Du, and R. H. Liu, "Physical Reservoir computing using magnetic skyrmion memristor and spin torque nano-oscillator," *Applied Physics Letters*, vol. 115, no. 19, p. 192403, 2019.